Empirical Scatter Correction using the Epipolar Consistency Condition

Mathis Hoffmann, Tobias Würfl, Nicole Maaß, Frank Dennerlein, André Aichert and Andreas K. Maier

***Abstract*—Scatter affects every computed tomography (CT) image. Calibration-free software scatter reduction methods have not been used extensively in practice. Recently, consistency conditions have been applied successfully to other artifact reduction problems in CT imaging. We propose a scatter reduction method, that uses an epipolar consistency condition (ECC) to estimate parameters of an additive scatter model. We evaluate our approach by comparing it with an image-based empirical scatter correction method (ESC) that uses the same scatter model. We show that it performs equally well on simulated data. Further, ECC outperforms ESC regarding the computational load for the determination of the parameter models, because ECC is formulated in projection domain such that no image reconstruction is necessary. While some restrictions might apply for the stability of ECC on measured data, no prior information needs to be formulated regarding the reconstructed image, like it is required with ESC.**

I. Introduction

Scatter is caused by two different physical effects [1]. On the one hand, photons are scattered (change their direction) at particles that are much smaller than the wavelength of the radiation. This is known as Rayleigh scattering. On the other hand, the Compton effect describes incoherent scattering, where a scattered photon looses energy, increasing its wavelength. These effects contradict the assumption of reconstruction algorithms that the measured radiation solely consists of primary radiation. Therefore, the image quality is reduced. To weaken the effect, hardware- and software-based scatter reduction methods are applied [2].

Reference-less software methods aim to estimate the scatter radiation using a suitable scatter model and a cost function to estimate its parameters. Monte Carlo simulations are the well known gold standard to estimate the scatter component precisely. However, the simulation is computationally demanding. The situation can be improved by performing a very coarse Monte Carlo simulation and using the result to fit a scatter model [3]. Alternatively, a scatter model can be fitted by optimization of a cost function in image domain, for example by the minimization of the total variation (TV). Meyer et. al [4] show that this is possible without successive reconstruction steps by exploiting the linearity of the Radon transform.

M. Hoffmann, T. Würfl and A. K. Maier are with the Pattern Recognition Lab, Friedrich-Alexander-Universität Erlangen-Nürnberg (FAU), Erlangen, Germany.
N. Maaß and F. Dennerlein are with Siemens Healthcare GmbH, Erlangen, Germany.

Recently, a new consistency condition based on redundant plane integrals was presented [5], [6] and has been successfully applied for geometry calibration [6], [7], motion compensation [8] and beam-hardening reduction [9].

We derive an algorithm using the epipolar consistency condition to estimate the parameters of a scatter model. The model we use was introduced by Ohnesorge et. al [10] and modified by Meyer et. al [4] to take the form of a linear combination. We exploit the results of Würfl et. al [9] to derive a closed-form solution that can be computed efficiently.

II. Methodology

In section II-A, we detail the model that we use to estimate the scatter component. In section II-B, we derive a closed-form solution to the estimation problem that uses the ECC as a cost function. In section II-C, we point at some insights that we gained from the model.

A. Model

Throughout this paper, we assume that scatter can be reduced using the additive model in line integral domain, that has been used by Meyer et. al [4]. The scatter-reduced raw-data $\boldsymbol{p}$ is given by

$$\boldsymbol{p} = \boldsymbol{q} - \sum_{n=1}^{N} w_n \boldsymbol{s}_n, \tag{1}$$

where $\boldsymbol{q}$ denotes the measured raw data. We need to estimate the raw-data scatter components $\boldsymbol{s}_n$ along with the weights w_n.

As the source for scatter resides in intesity domain, we need to estimate the scatter intensity $I_{\boldsymbol{s}}$ to obtain the scatter components $\boldsymbol{s}_n$. The scatter intensity consists of an intensity model $I_{\boldsymbol{f}}$ that is convolved with a model for the scatter point spread function. The intensity model is given by

$$I_{\boldsymbol{f}} = \alpha \boldsymbol{p} I_{\boldsymbol{p}}, \tag{2}$$

where $I_{\boldsymbol{p}} = e^{-\boldsymbol{p}}$ and α is a scale parameter that depends on the scatter cross section. From $I_{\boldsymbol{f}}$, the scatter component in intensity domain can be calculated as

$$I_{\boldsymbol{s}} = I_{\boldsymbol{f}} * \left[\exp\left(\frac{x+\beta}{\gamma}\right) + \exp\left(\frac{x-\beta}{\gamma}\right) \right], \tag{3}$$

where β and γ determine the shape of the scatter point spread function and x denotes the spatial location on the detector.

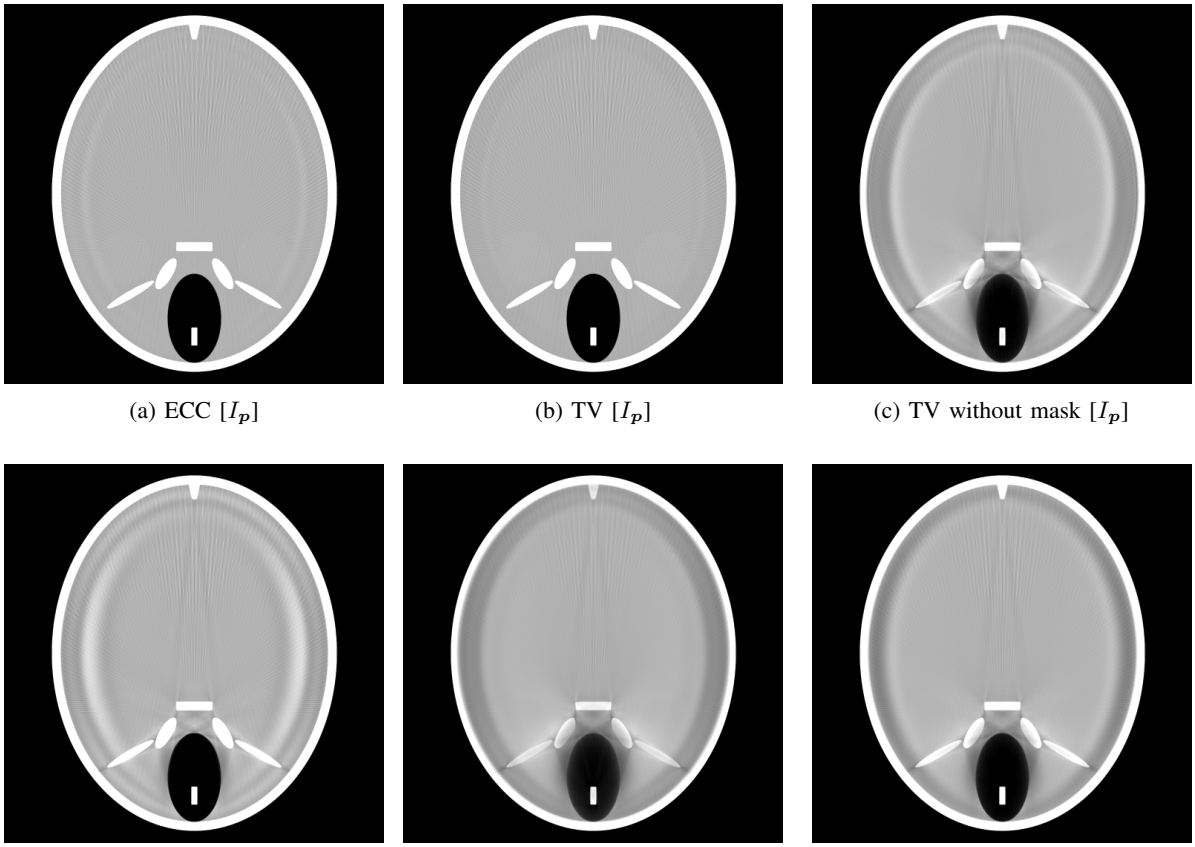

(a) ECC [$I_{\boldsymbol{p}}$] (b) TV [$I_{\boldsymbol{p}}$] (c) TV without mask [$I_{\boldsymbol{p}}$]

(d) ECC [$I_{\boldsymbol{q}}$] (e) TV [$I_{\boldsymbol{q}}$] (f) $I_{\boldsymbol{q}}$ - Uncorrected

Fig. 1: Results for the inverse crime scenario using the the proposed ECC-based method and the TV-based approach. The notation [$I_{\boldsymbol{p}}$] denotes that the ideal projection data has been used to generate the scatter components (see Eq. (2)), whereas [$I_{\boldsymbol{q}}$] denotes that the projection with simulated scatter has been used instead.

To enable a linear estimation using the ECC, we obtain the scatter component in line integral domain by

$$\begin{aligned}\boldsymbol{s} &= -\ln\left(I_{\boldsymbol{s}} + I_{\boldsymbol{p}}\right) + \ln\left(I_{\boldsymbol{p}}\right) \\ &= -\ln\left(\frac{I_{\boldsymbol{s}}}{I_{\boldsymbol{p}}} + 1\right).\end{aligned} \tag{4}$$

Eq. (1) already indicates that we use N of those scatter components to find the scatter-free image $\boldsymbol{p}$. We denote a specific scatter component that is obtained from parameters $(\alpha_n,\, \beta_n,\, \gamma_n)$ as $\boldsymbol{s}_n$. Note that this model assumes that the ideal, scatter-free data $I_{\boldsymbol{p}}$ is known to create the scatter components. This is generally not the case. A common solution is to apply any algorithm relying on this model in a fixed-point iteration scheme. Throughout the following, we only consider a single iteration of this algorithm.

B. Estimation

Given two X-ray projections, any plane which contains both source positions intersects the detectors in so-called corresponding epipolar lines. Epipolar consistency states that the derivative orthogonal to their common plane is identical in either image:

$$\frac{\partial}{\partial \boldsymbol{t}} \rho_{\boldsymbol{p}_0}\left(\boldsymbol{l}_0\right) = \frac{\partial}{\partial \boldsymbol{t}} \rho_{\boldsymbol{p}_1}\left(\boldsymbol{l}_1\right). \tag{5}$$

Here, $(\rho_{\boldsymbol{p}_0},\, \rho_{\boldsymbol{p}_1})$ denotes the Radon transform of a pair of projection images $(\boldsymbol{p}_0,\, \boldsymbol{p}_1)$, $(\boldsymbol{l}_0,\, \boldsymbol{l}_1)$ denote intersection lines of an epipolar plane with the corresponding detector planes and $\frac{\partial}{\partial \boldsymbol{t}}$ denotes the derivative of the Radon transformed projections perpendicular to the lines.

We combine the additive scatter model (Eq. (1)) with Eq. (5) to receive

$$\frac{\partial}{\partial \boldsymbol{t}} \rho_{\left(\boldsymbol{q}_0 - \sum_{n=1}^{N} w_n \boldsymbol{s}_{n,0}\right)}\left(\boldsymbol{l}_0\right) = \frac{\partial}{\partial \boldsymbol{t}} \rho_{\left(\boldsymbol{q}_1 - \sum_{n=1}^{N} w_n \boldsymbol{s}_{n,1}\right)}\left(\boldsymbol{l}_1\right), \tag{6}$$

where $(\boldsymbol{s}_{n,0},\, \boldsymbol{s}_{n,1})$ are the n'th scatter components of the projection image pair $(\boldsymbol{q}_0,\, \boldsymbol{q}_1)$. Because the Radon transform and the derivative operator are linear, we reuse the idea of epipolar consistency guided beam hardening reduction [9] and rewrite Eq. (6) to

$$\boldsymbol{q}_0'\left(\boldsymbol{l}_0\right) - \sum_{n=1}^{N} w_n \boldsymbol{s}_{n,0}'\left(\boldsymbol{l}_0\right) = \boldsymbol{q}_1'\left(\boldsymbol{l}_1\right) - \sum_{n=1}^{N} w_n \boldsymbol{s}_{n,1}'\left(\boldsymbol{l}_1\right), \tag{7}$$

where we substituted $\boldsymbol{q}_i' = \frac{\partial}{\partial \boldsymbol{t}} \rho_{\boldsymbol{q}_i}$ and $\boldsymbol{s}_{n,i}' = \frac{\partial}{\partial \boldsymbol{t}} \rho_{\boldsymbol{s}_{n,i}}$, $i \in [0, 1]$. Unfortunately, the scatter components $\boldsymbol{s}_n$ are not linear in the parameters (see Eqs. (2), (3) and (4)). Therefore, we follow the idea from empirical scatter correction [4], generate N different estimates of the scatter components and

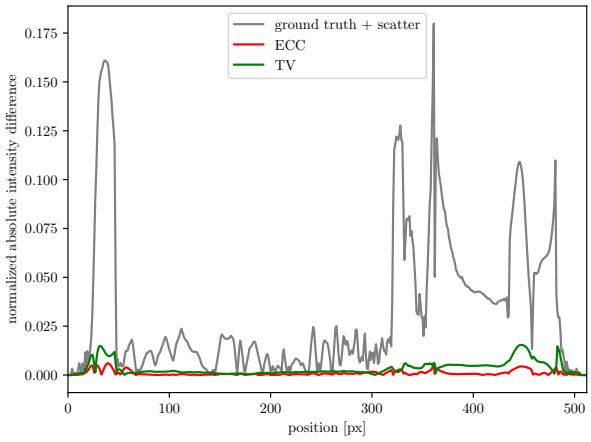

(a) $[I_{\boldsymbol{p}}]$

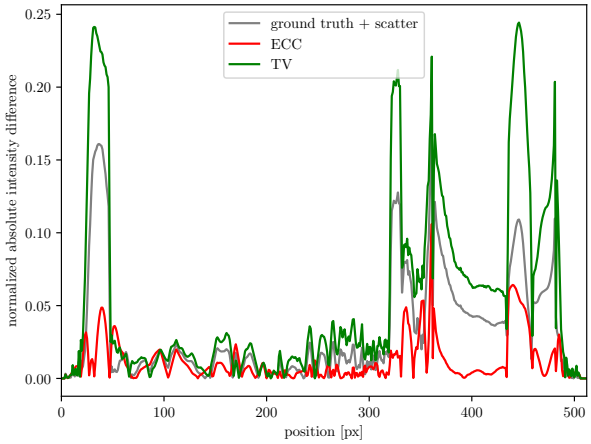

(b) $[I_{\boldsymbol{q}}]$

Fig. 2: Normalized absolute intensity difference of line profiles to the ground truth.

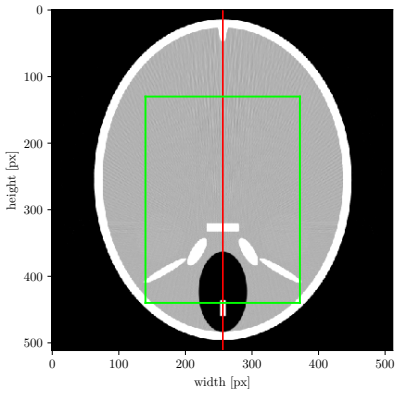

Fig. 3: Region (green) that has been used to estimate SSIM and PSNR (see Fig. 4) and line (red) along which the profiles have been calculated.

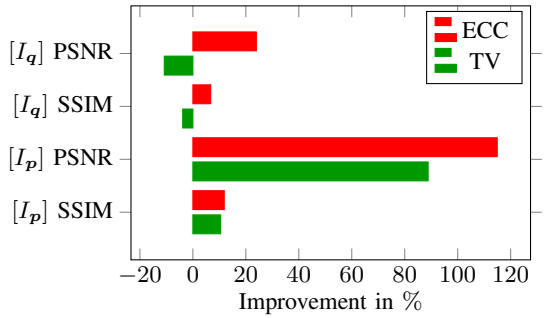

Fig. 4: Performance of our (ECC) and the TV-based method in terms of PSNR and SSIM. 0% improvement means that there is no improvement over the volume with simulated scatter. The measures have been computed in 2D within the region depicted in Fig. 3.

assume that they behave as a basis for the space of scatter components. In section II-C, we point out, that this approach has theoretical drawbacks. However, our experiments (section III) reveal that it performs well in practice.

In order to estimate the coefficients w_n, we optimize for consistency, such that the scatter components remain constant:

$$\min \left[\left(\sum_{n=1}^{N} w_n \boldsymbol{s}'_{n,0}\left(\boldsymbol{l}_0\right) - \boldsymbol{s}'_{n,1}\left(\boldsymbol{l}_1\right) \right) - \boldsymbol{q}'_0\left(\boldsymbol{l}_0\right) - \boldsymbol{q}'_1\left(\boldsymbol{l}_1\right) \right]^2 . \tag{8}$$

So far, we stated the problem for $(\boldsymbol{l}_0, \boldsymbol{l}_1)$, which corresponds to one epipolar plane and one pair of projection images. We want to solve this problem for K planes $\boldsymbol{l}^k_{p,i}$ across P pairs of projection images. Therefore, we have $M = PK$ measurements, producing an overdetermined system of linear equations:

$$\hat{\boldsymbol{w}} = \arg\min_{\boldsymbol{w}} \|\boldsymbol{A}\boldsymbol{w} - \boldsymbol{b}\|_2^2 \tag{9}$$

where

$$\boldsymbol{A} = \begin{bmatrix} a_{1,1,1} & \dots & a_{1,1,N} \\ \vdots & \ddots & \vdots \\ a_{1,K,1} & \dots & a_{1,K,N} \\ a_{2,1,1} & \dots & a_{2,1,N} \\ \vdots & \ddots & \vdots \\ a_{P,K,1} & \dots & a_{P,K,N} \end{bmatrix}$$

with

$$a_{p,k,n} = \boldsymbol{s}'_{n,p,0}\left(\boldsymbol{l}^k_{p,0}\right) - \boldsymbol{s}'_{n,p,1}\left(\boldsymbol{l}^k_{p,1}\right)$$

and

$$\boldsymbol{b} = \left[b_{1,1}, \dots, b_{1,K}, b_{2,1}, \dots, b_{P,K}\right]^\top$$

with

$$b_{p,k} = \boldsymbol{q}'_{p,0}\left(\boldsymbol{l}^k_{p,0}\right) - \boldsymbol{q}'_{p,1}\left(\boldsymbol{l}^k_{p,1}\right).$$

Note that the columns of $\boldsymbol{A}$ are linearly independent. Therefore, the solution to Eq. (9) is given by

$$\hat{\boldsymbol{w}} = (\boldsymbol{A}^\top \boldsymbol{A})^{-1} \boldsymbol{A}^\top \boldsymbol{b} = \boldsymbol{A}^+ \boldsymbol{b}. \tag{10}$$

C. Discussion

Typically, such linear combinations of basis images are applied in the domain where the artifact arises. However, this model using scatter basis functions in line integral domain is not equal to a linear combination of scatter basis functions in intensity domain (see Eq. (1)). To investigate this, we transform the linear combination $\sum_n w_n \boldsymbol{s}_n$ to intensity domain:

$$\sum_n w_n \ln\left(I_{\boldsymbol{s},n}\right) = \sum_n \ln\left(I_{\boldsymbol{s},n}^{w_n}\right) = \ln\left(\prod_n I_{\boldsymbol{s},n}^{w_n}\right). \quad (11)$$

This result shows that the linear combination in raw data domain does not correspond to a linear combination in intensity domain.

III. Experiments

We present two simulation experiments using the Forbild head phantom. We show the performance of the proposed algorithm in two inverse crime scenarios and compare the results to the method proposed by Meyer et. al that minimizes the total variation in volume domain, instead of the epipolar consistency in projection domain.

A. Setup

For the experiments, we define a feasible parameter range $\beta \in \left[\beta_l = 1\mathrm{e}^{-2},\, \beta_u = 1.5\mathrm{e}^{-2}\right]$, $\gamma \in \left[\gamma_l = \mathrm{e}^{-3},\, \gamma_u = 1\mathrm{e}^{-2}\right]$. The parameter α remains fixed at $\alpha = 4\mathrm{e}^{-10}$. We use $N = 4$ scatter basis images such that $(\beta_n,\, \gamma_n) \in (\beta_l,\, \beta_u) \times (\gamma_l,\, \gamma_u)$. The simulated scatter image is generated with $\beta_{\text{sim}} = 1.2\mathrm{e}^{-2}$, $\gamma_{\text{sim}} = 8\mathrm{e}^{-3}$. For the first simulation experiment, we generate the scatter components using the ideal projection intensity $I_{\boldsymbol{p}}$ (see Eq. (2)). The results of this experiment are annotated with $[I_{\boldsymbol{p}}]$. For the second simulation experiment, we use the projection intensity with simulated scatter $I_{\boldsymbol{q}}$ for the scatter components and annotate the results with $[I_{\boldsymbol{q}}]$.

B. Results

The results of our experiments are summarized in Fig. 1. We find, that both methods yield visually comparable results when $I_{\boldsymbol{p}}$ is used to generate the scatter components (Figs. 1a and 1b). However, both methods produce worse results, when $I_{\boldsymbol{q}}$ is used instead (Figs. 1c and 1d).

Fig. 2 depicts, how a line profile through the scatter-reduced volumes differs from the line profile through the ground-truth volume. For the case where the scatter components are based on $I_{\boldsymbol{p}}$, the results for both methods only differ slightly. Notably, there is an advantage for the ECC-based parameter estimation in the frontal sinus area within the phantom. This is due to a mandatory masking of soft- and hard-tissue regions in the TV-based approach (see also Fig. 1c) that eliminates contributions from regions with low attenuation to the loss. For the case where the scatter components are based on $I_{\boldsymbol{q}}$, worse results can be seen in both methods.

Finally, we compare the structure similarity (SSIM) and peak signal noise ratio (PSNR) of the scatter-reduced slices. The results are shown in Fig. 4. Regarding these measures, the ECC-based parameter estimation is superior to the TV-based approach in all cases.

IV. Conclusion

We have presented a novel reference-free scatter reduction algorithm and showed that it improves over a similar algorithm in terms of achievable image quality and computational efficiency. Overall, the PSNR is about 35% better, whereas the SSIM is also slightly better, compared to the reference algorithm. The estimation of the weights with our method happens to be 52 times faster using an unoptimized numerical Python implementation.

A key advantage of using a consistency condition is, that it does not impose any assumption about the object. We reuse the scatter reduction model from Meyer et. al to obtain a computationally efficient formulation of the optimization problem on intermediate functions in line integral domain with a closed-form solution. However, we show that this mathematical model has disadvantageous physical properties. Still we found the algorithm works well in simulation experiments, even if we restrict ourselves to a single iteration of the algorithm. In future work we want to evaluate the algorithm extensively on measured data. Additionally we want to explore different scatter reduction models better modeling the physical properties while preserving computational efficiency.

Acknowledgment

A. Aichert is supported by the German Research Foundation; DFG MA 4898/3-1.

Disclaimer

The concepts and information presented in this paper are based on research and are not commercially available.

References

[1] P. M. Joseph and R. D. Spital, "The effects of scatter in x-ray computed tomography," *Med. Phys.*, vol. 9, no. 4, pp. 464–472, 1982.

[2] E.-P. Rührnschopf and K. Klingenbeck, "A general framework and review of scatter correction methods in x-ray cone-beam computerized tomography. part 1: Scatter compensation approaches," *Med. Phys.*, vol. 38, no. 7, pp. 4296–4311, 2011.

[3] M. Baer and M. Kachelrieß, "Hybrid scatter correction for ct imaging," *Phys. in Med. and Bio.*, vol. 57, no. 21, p. 6849, 2012.

[4] E. Meyer, C. Maaß, M. Baer, R. Raupach, B. Schmidt, and M. Kachelrieß, "Empirical scatter correction (esc): A new ct scatter correction method and its application to metal artifact reduction," in *Nuclear Science Symposium Conference Record (NSS/MIC), 2010 IEEE*. IEEE, 2010, pp. 2036–2041.

[5] C. Debbeler, N. Maass, M. Elter, F. Dennerlein, and T. M. Buzug, "A new CT rawdata redundancy measure applied to automated misalignment correction," in *12th Int. Meet. Fully 3D Reconstr. Radiol. Nucl. Med*, 2013, pp. 264–267.

[6] A. Aichert, M. Berger, J. Wang, N. Maass, A. Doerfler, J. Hornegger, and A. K. Maier, "Epipolar consistency in transmission imaging," *IEEE Trans. Med. Imaging*, vol. 34, no. 11, pp. 2205–2219, 2015.

[7] N. Maass, F. Dennerlein, A. Aichert, and A. Maier, "Geometrical jitter correction in computed tomography," in *3rd Int. Conf. on image formation in X-ray computed tomography, edited by Frederic Noo, Salt Lake City*, 2014, pp. 338–342.

[8] M. Unberath, A. Aichert, S. Achenbach, and A. Maier, "Consistency-based respiratory motion estimation in rotational angiography," *Med. Phys.*, vol. 44, no. 9, 2017.

[9] T. Würfl, N. Maass, F. Dennerlein, X. Huang, and A. Maier, "Epipolar consistency guided beam hardening reduction - ECC^2," in *14th Int. Meet. Fully 3D Reconstr. Radiol. Nucl. Med*, 2017, pp. 181–185.

[10] B. Ohnesorge, T. Flohr, and K. Klingenbeck-Regn, "Efficient object scatter correction algorithm for third and fourth generation ct scanners," *European radiology*, vol. 9, no. 3, pp. 563–569, 1999.